NANO LETTERS

pubs.acs.org/NanoLett Letter

Nanocrystal Ordering Enhances Thermal Transport and Mechanics in Single-Domain Colloidal Nanocrystal Superlattices

Zhongyong Wang,[⊥] Alexander D. Christodoulides,[⊥] Lingyun Dai, Yang Zhou, Rui Dai, Yifei Xu, Qiong Nian, Junlan Wang, Jonathan A. Malen, and Robert Y. Wang*

Cite This: *Nano Lett.* 2022, 22, 4669−4676 Read Online

ACCESS | Metrics & More | Article Recommendations | Supporting Information

ABSTRACT: Colloidal nanocrystal (NC) assemblies are promising for optoelectronic, photovoltaic, and thermoelectric applications. However, using these materials can be challenging in actual devices because they have a limited range of thermal conductivity and elastic modulus, which results in heat dissipation and mechanical robustness challenges. Here, we report thermal transport and mechanical measurements on single-domain colloidal PbS nanocrystal superlattices (NCSLs) that have long-range order as well as measurements on nanocrystal films (NCFs) that are comparatively disordered. Over an NC diameter range of 3.0−6.1 nm, we observe that NCSLs have thermal conductivities and Young's moduli that are up to ∼3 times higher than those of the corresponding NCFs. We also find that these properties are more sensitive to NC diameter in NCSLs relative to NCFs. Our measurements and computational modeling indicate that stronger ligand−ligand interactions due to enhanced ligand interdigitation and alignment in NCSLs account for the improved thermal transport and mechanical properties.

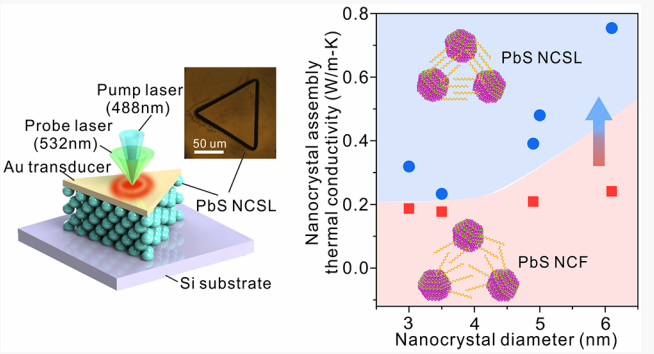

KEYWORDS: *nanocrystal, superlattice, ligands, thermal transport, mechanics*

Colloidal nanocrystals (NCs) consist of inorganic crystalline cores protected by a layer of surface-bound molecules (ligands). Interparticle interactions facilitate NC self-assembly into materials commonly called NC solids, which have tunable electrical and optical properties that are promising for electronics,[1−6] optoelectronics,[2,5,7] photovoltaics,[5−8] and thermoelectrics.[6,9−11] Thermal transport and mechanical properties are also important because these devices must meet thermal management and mechanical robustness demands. However, NC solids generally have limited thermal conductivities (0.1 to 0.4 W m^{-1} K^{-1}) and elastic moduli (30 MPa to 1 GPa) due to the weak van der Waals (vdW) interactions between the ligands of adjacent NCs.[12,13] Previous work focused on modifying NC surface chemistry to improve these properties. Ong et al.[12] and Liu et al.[14] showed that the thermal transport is insensitive to the NC core material and sensitive to the ligand material and volume fraction. Furthermore, our recent work[15] on iron oxide NC solids demonstrates that cross-linking ligands simultaneously increases the thermal conductivity and Young's modulus.

Prior work reported that ligands on adjacent NC cores interact with each other via vdW interactions.[16−20] This is similar to the vdW interaction between polymer chains, and standard polymers do indeed have thermal conductivities and Young's moduli similar to those of NC solids. However, improving the polymer chain alignment has been shown to significantly increase the thermal conductivity and mechanical strength.[21−23] Several theoretical[24] and experimental[25−27] studies have also shown that planar self-assembled monolayers (SAMs) of aligned hydrocarbon chains can exhibit high thermal conductance. The ligands on colloidal NCs bear some resemblance to polymers and SAMs, but with added complexity originating from curved surfaces, three-dimensional assemblies, and processing methods.[28,29] Whether the concept of enhancing thermal transport and mechanics via ligand alignment applies to NC assemblies remains unknown.

Early work[30−34] demonstrated that disordered nanocrystal films (NCFs) and long-range ordered nanocrystal superlattices (NCSLs) can be prepared by quick solvent evaporation and slow nonsolvent diffusion, respectively. The long-range ordering in NCSLs is facilitated by slow formation, during which NCs rearrange to achieve enhanced ligand−ligand interactions. The precise structure of NCSLs is determined by a rich phase

Received: February 10, 2022
Revised: May 20, 2022
Published: May 31, 2022

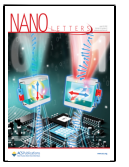

https://doi.org/10.1021/acs.nanolett.2c00544
Nano Lett. 2022, 22, 4669−4676

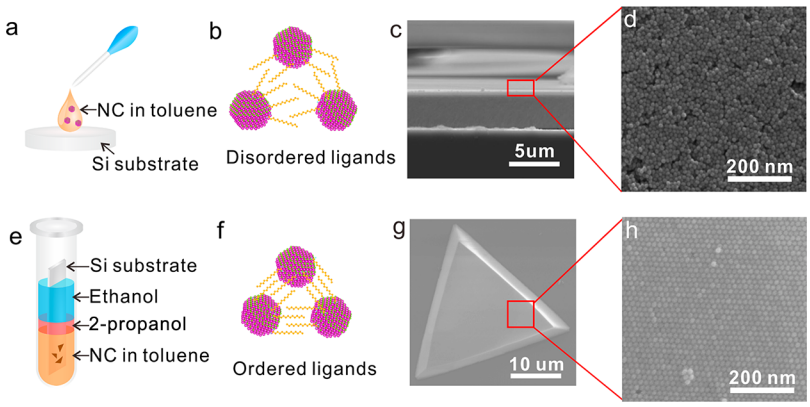

Figure 1. Materials characterizations of a randomly packed PbS nanocrystal film (NCF) and a long-range ordered PbS nanocrystal superlattice (NCSL): (a) schematic illustration for quick drying of a nanocrystal (NC) solution via drop-casting or spin-coating; (b) schematic of adjacent NCs with disordered ligand packing when the solvent quickly evaporates; (c) cross-sectional SEM image of a spin-coated NCF; (d) high-resolution SEM image of spin-coated NCs illustrating the disordered packing of PbS NCs; (e) schematic illustration for controlled destabilization of an NC solution via slow diffusion of a nonsolvent through a buffer layer (i.e., ethanol through 2-propanol); (f) schematic of adjacent NCs with ordered ligand packing when the NC solution is slowly destabilized by nonsolvent diffusion; (g) SEM image of a triangular-shaped single-domain NCSL prepared using the nonsolvent diffusion method; (h) High-resolution SEM image of a NCSL showing ordered packing of PbS NCs in a single-domain NCSL. We note that larger ∼10 nm NCs were used to achieve the single-NC resolution in parts (d) and (h) of this figure. However, we also found that these larger diameters generally yielded smaller NCSLs that were insufficient for measurements.

behavior that depends on intercoupled parameters such as ligand type,[35,36] ligand coverage density,[37] NC size,[20,38,39] NC shape/faceting,[40] and NCSL growth/processing.[3,30,31] NCSLs most commonly adopt a face-centered-cubic phase,[39,41,42] and under certain conditions the NCs can exhibit an orientational atomic alignment[42,43] with one another. This study focuses on the specific case of PbS NCs with oleic acid (OA) ligands. The kinked OA molecular structure permits many ligand−ligand configurations ranging from minimal interdigitation (coiled structures) to partial interdigitation up to the C═C double-bond of the OA backbone.[36,44] For the purposes of this letter, we broadly use the term "ligand interdigitation" to refer to the amount of overlap between the ligand shells of adjacent NCs. We also use the term "ligand order" to refer to the alignment/parallelism of the carbon backbones between adjacent ligands. At a basic level, this ligand alignment/parallelism can in turn be related to the NC surface curvature (and at a deeper level can be further related to the NC faceting/shape).

In this work, we demonstrate that long-range ordering in NC superlattices leads to a several-fold improvement in thermal conductivity and Young's modulus in comparison to NCFs. We also find that these properties are more sensitive to the NC diameter in NCSLs relative to NCFs. We measured the thermal conductivity and Young's modulus using frequency domain thermoreflectance and nanoindentation. We complement these measurements with coarse-grained modeling, atomistic molecular dynamics (MD), and effective medium approximation (EMA) modeling. These experimental measurements and computational models indicate that the enhanced ligand interdigitation and alignment in NCSLs leads to the improved properties.

We synthesized monodisperse 3.0−6.1 nm PbS NCs with OA ligands using a modified Hines method.[45] NCFs and NCSLs were characterized with scanning electron microscopy (SEM), transmission electron microscopy (TEM), and atomic force microscopy (AFM). TEM images (Figure S1) show that the NCs are approximately spherical and uniform in size. In addition, these images show that the NCs have an interparticle spacing of ∼1.5 nm (where interparticle spacing refers to the edge-to-edge spacing between nearest-neighbor NC cores). This interparticle spacing originates from a bilayer of OA ligands that are attached to the neighboring NC surfaces. Figure 1a−d shows that spin-coating an NC solution results in smooth NCFs (Figure S3 shows additional images and data). NCFs feature a disordered ligand arrangement and NC packing, and consequently larger interparticle spacings and weaker ligand−ligand interactions. This is because the fast-solvent evaporation during deposition prevents the NCs and ligands from fully rearranging into their most thermodynamically favorable state. In contrast, Figure 1e−h shows that destabilizing an NC solution through slow diffusion of a nonsolvent leads to highly ordered single-domain NCSLs of triangular or hexagonal shape (Figure S2 shows additional images and data). A high-resolution SEM image of a NCSL shows that the NCs are well-ordered within the superlattice structure (Figure 1h).

The differences in interparticle spacing between NCSLs and NCFs has been characterized by Lee et al.[46] using small-angle X-ray scattering. They found that internanocrystal spacings in NCSLs decrease by ∼20% relative to disordered NCFs. This spacing decrease occurs because, during the weeks-long NCSL formation process, the NCs freely reorient to achieve better ligand interdigitation and more effectively reach their most thermodynamically favorable state. On the basis of our measured 1.5 nm interparticle spacings and this reported 20% difference,[46] we use an interparticle spacing of 1.2 nm for our NCSL analyses.

We measured the thermal conductivities of NCSLs and NCFs using frequency domain thermoreflectance (Figure 2a and Section V of the Supporting Information).[12,26,47] All samples had a 70 nm thick Au transducer layer predeposited with electron-beam evaporation. This 70 nm thickness was chosen to balance requirements for optical opacity (thicker is better) and cross-plane thermal transport (thinner improves measurement sensitivity). The sample was then periodically heated with an intensity-modulated pump laser (λ = 488 nm), while it was simultaneously probed by a secondary laser (λ = 532 nm). The sample's periodic thermal response to the pump

https://doi.org/10.1021/acs.nanolett.2c00544
Nano Lett. 2022, 22, 4669−4676

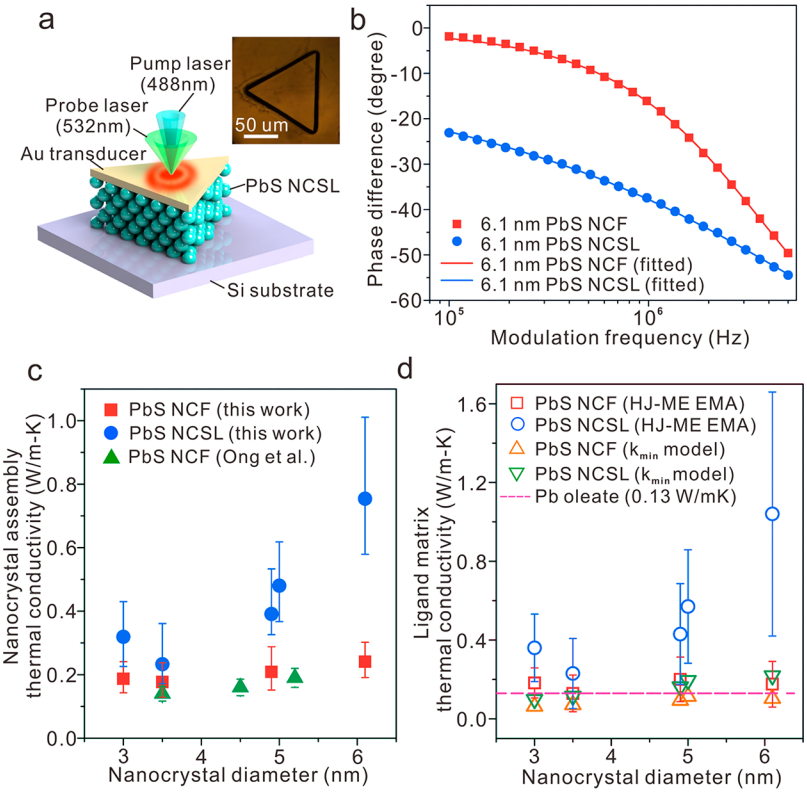

Figure 2. Thermal conductivity measurements and effective medium approximation (EMA) modeling of PbS nanocrystal superlattices (NCSLs) and nanocrystal films (NCFs) for various nanocrystal (NC) diameters. (a) Schematic illustration of a thermal conductivity measurement on an Au-coated PbS NCSL using frequency domain thermoreflectance (FDTR). The inset shows an optical microscope image of a representative Au-coated PbS NCSL. (b) Representative data for the FDTR phase difference versus pumping frequency showing excellent agreement between the experimental data and theoretical fits for both NCSLs and NCFs. (c) Thermal conductivity of PbS NCSLs and NCFs of various core sizes. Previous measurements on PbS NCFs by Ong et al.[12] using the same technique are included as a benchmark and demonstration of consistency. Lower and upper error bars represent the 10th and 90th quantiles of fit distributions gathered by a Monte Carlo estimation of uncertainty, respectively. (d) Ligand matrix thermal conductivity interpreted from the Hasselman–Johnson–Maxwell–Euken (HJ-ME) EMA model and corresponding comparisons with the minimum thermal conductivity (k_{min}) model and thermal conductivity of Pb-oleate wax.

laser is measured via its temperature-dependent reflectivity (i.e., thermoreflectance). The phase difference of temperature (probe) and heat flux (pump) is fitted to a heat diffusion equation solution to determine the thermal conductivity.[48] A sensitivity analysis (Figure S13b) shows that our measurement is insensitive to the heat capacity and NCSL thickness input parameters. Other parameters to which the measurement is more sensitive, namely the laser spot size and the Au transducer thermal conductivity, are well-controlled across all NC diameters to ensure accurate fitting. Figure 2b shows that the experimental phase difference accurately fits the theoretical model over a broad frequency range.

Our results show that the thermal conductivities of NCSLs consistently exceed those of NCFs (Figure 2c). The thermal conductivity of NCFs increases from 0.19 ± 0.05/−0.04 to 0.24 ± 0.06/0.05 W m^{-1} K^{-1} as the NC diameter increases from 3.0 to 6.1 nm, which agrees with previous reports.[12,14] NCSLs have thermal conductivities that are up to ∼3 times higher than those of NCFs over this same diameter range (0.32 ± 0.11/0.09 to 0.75 ± 0.26/0.18 W m^{-1} K^{-1}). We also find that the NCSL thermal conductivity is more sensitive to the diameter in comparison to NCFs, with increasing thermal conductivity enhancements for larger diameters. The magnitude of this increase is similar to that achieved in cross-linked versus non-cross-linked iron oxide NCs,[15] but is particularly notable due to its differing mechanism. Unlike the strong covalent bonds formed in cross-linked iron oxide NCs, PbS NCSLs still feature weak vdW interactions. Moreover, the ligand cross-linking approach used for iron oxide NCs requires a high-temperature 350 °C annealing process that is incompatible with many NC materials. In contrast, this approach of using NC ordering to improve thermal transport is more generalizable across NC materials.

To better understand the origins of the increased thermal conductivity, we performed Young's modulus measurements of the NCFs and NCSLs using nanoindentation (Section II of the Supporting Information). Classical kinetic theory relates thermal conductivity to the volumetric heat capacity (C), average phonon velocity ($\overline{v}$), and average phonon mean free path ($\overline{l}$) via the relation $k = C\overline{v}\overline{l}/3$. This relationship allows us to qualitatively assess the relative contributions of C, $\overline{v}$, and $\overline{l}$ to the thermal conductivity. In addition, the average phonon velocity can be approximated as the average speed of sound, $\overline{v}_s$. In this manner, the thermal conductivity and Young's modulus can be linked via the sound speed because $v_s \propto \sqrt{E/\rho}$, where E and ρ are the Young's modulus and density, respectively.

Our nanoindentation results indicate that NCSLs have a Young's modulus up to ∼3 times higher than NCFs (Figure 3f). This variance can be ascribed to varied ligand–ligand interactions, as illustrated in Figure 3a,b for NCFs and NCSLs, respectively. Representative indents on NCFs and NCSLs are shown in Figure 3c,d, respectively. The Young's moduli of both

https://doi.org/10.1021/acs.nanolett.2c00544
Nano Lett. 2022, 22, 4669−4676

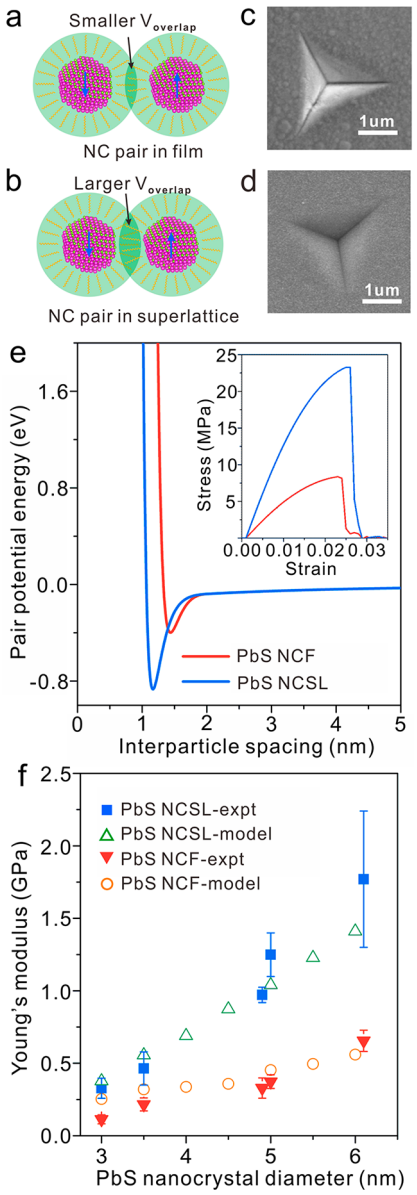

Figure 3. Mechanical property measurements and coarse-grained model simulation of nanocrystal films (NCFs) and nanocrystal superlattices (NCSLs). Schematic illustration of a nanocrystal (NC) pair with (a) weaker and (b) stronger ligand−ligand interaction in NCFs and NCSLs, respectively. Accompanying this weaker and stronger ligand−ligand interaction are smaller and larger overlap volumes of the ligand shells, $V_{overlap}$. SEM images of representative nanoindentations on a (c) PbS NCF and (d) PbS NCSL, respectively. (e) NC pair potentials for a 6 nm PbS NCF and a 6 nm PbS NCSL. The inset shows the calculated stress−strain curves of three-dimensional NC assemblies using the different pair potentials and corresponding coarse-grained models. (f) Young's modulus of PbS NCFs and NCSLs of various core sizes measured with nanoindentation (closed symbols) along with results fitted to the stress−strain curves generated by the coarse-grained model (open symbols). The stress−strain curves generated via the coarse-grained model are shown in the inset of (e) as well as in Figures S8 and S9.

NCFs and NCSLs increase ∼5-fold as the diameter increases from 3.0 to 6.1 nm. We attribute this diameter dependence to two effects. First, the increased volume fraction of "stiff" NC cores relative to "soft" ligand matrices should partially contribute to this trend. Second, the alignment and interdigitation of molecular ligands are expected to improve as the diameter increases (i.e., surface curvature decreases),[28,49] and this should improve the ligand matrix's mechanical properties. Figure 3f also shows that NCSLs have a steeper rate of Young's modulus increase with diameter in comparison to NCFs. We attribute this to a dampening of the surface curvature effect in disordered NCFs relative to ordered NCSLs. We also observed that NCSLs were harder than NCFs (Figure S5).

To gain insight into the differences between NCSLs and NCFs, we employed pair potential and three-dimensional coarse-grained models (Section III of the Supporting Information). We describe the interaction between two neighboring NCs by fitting the equilibrium interparticle spacings (1.5 and 1.2 nm for NCFs and NCSLs, respectively) to a pair potential model. This pair potential has three major components: the vdW attraction between the NC cores, dipole−dipole interactions, and ligand−ligand interactions.[50] Figure S6 shows each component's contribution and demonstrates that the ligand−ligand interaction is more pronounced in NCSLs than in NCFs. We next used this pair potential to build a coarse-grained three-dimensional NCSL in a face-centered cubic lattice and derive mechanical properties using a "stress−strain" method.

As was discussed earlier, NCSLs feature narrower interparticle spacing and thus better ligand interdigitation. Figure 3e shows that, by specifying an equilibrium position shift from 1.5 nm (NCF) to 1.2 nm (NCSL), the potential is lower and steeper near the equilibrium position. This leads to a Young's modulus increase as based on stress−strain curves from 3D coarse-grained models (Figure 3e inset; see Figures S8 and S9 for additional data). Figure 3f shows that our coarse-grained simulations fit the experimental data well. This illustrates that ligand−ligand interactions (which are related to the overlap volume between adjacent NC ligand shells) have a key role in the mechanical properties. This increased overlap volume can also be related to the increased ligand order and interdigitation that occur in NCSLs. We also performed atomistic MD simulations that corroborate this ligand−ligand interdigitation effect on Young's modulus (Section IV of the Supporting Information).

Since the Young's modulus and thermal conductivity are interrelated via the speed of sound, we used our Young's modulus data to determine the average speed of sound (Section II of the Supporting Information). Figure 4a shows that the average sound speed in NCSLs is ∼40−60% larger than that in NCFs. While this increase in average sound speed boosts the thermal conductivity, it is by itself insufficient to explain the up to ∼3× enhancement in NCSLs.

The thermal conductivity of NCSLs and NCFs appear to be linearly related to the average sound speed, albeit with a steeper curve for NCSLs relative to NCFs (Figure 4b). This indicates that additional effects contribute to the thermal conductivity differences between NCSLs and NCFs. We measured the volumetric heat capacity (Figure S4c), since kinetic theory indicates that the thermal conductivity depends linearly upon this parameter. However, we found that the volumetric heat capacity difference between NCSLs and NCFs is too small to explain this thermal conductivity difference. Furthermore, the heat capacity decreases with increasing NC diameter, which trends opposite of the thermal conductivity data (Figure 2c). In theory, the periodicity of NCSLs could lead to coherent phonons that are absent in disordered NCFs.

https://doi.org/10.1021/acs.nanolett.2c00544
Nano Lett. 2022, 22, 4669−4676

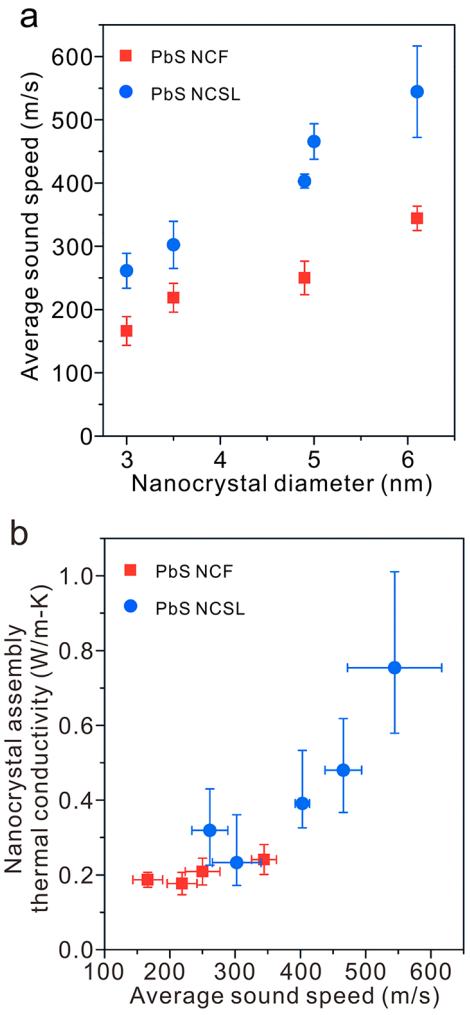

Figure 4. Sound speeds of colloidal PbS nanocrystal films (NCFs) and nanocrystal superlattices (NCSLs) and their corresponding relation to thermal transport. (a) Calculated average sound speeds on the basis of nanoindentation measurements for various nanocrystal (NC) core diameters. (b) NC assembly thermal conductivity as a function of average sound speed.

However, our analysis of coherent phonons in NCSLs indicate that the potential contribution of coherent phonons to the thermal conductivity is too small to be meaningful (Section VIII of the Supporting Information). In addition, our analysis shows that thermal conductivity contributions from coherent phonons would decrease with increasing diameter, and this also trends opposite of the thermal conductivity data (Figure 2c). Finally, kinetic theory states that the thermal conductivity also depends linearly on the average phonon mean free path (MFP). On the basis of the data in Figures 2c and 4, we conclude that both the sound speed and MFP increase with NC diameter. As the NC diameter increases (NC surface curvature decreases), the corresponding improved ligand alignment and interdigitation should increase the phonon MFP. This effect is likely more pronounced in ordered NCSLs and relatively muted in disordered NCFs. We note at this point that the NCSL samples in this study have only undergone a basic materials characterization and that we have assumed that our quasi-spherical PbS NCs are packed into a face-centered-cubic lattice.[39,41,42] A more detailed materials characterization combined with synthetic control over ligand capping density and NC faceting/shape could lead to variations in ligand interdigitation/order,[36,44] the orientational alignment of NCs,[42,43] alternative NCSL packing symmetries,[20,37] and other novel superlattice characteristics. While this level of analysis is beyond the scope of this letter, it also provides a rich landscape for future study.

Since NCFs and NCSLs are effectively composites consisting of NC particles dispersed in a ligand matrix, we employ the Hasselman–Johnson–Maxwell–Euken (HJ-ME) effective medium approximation (EMA) model to interpret the effects of the individual composite components on the overall thermal conductivity (Section VI of the Supporting Information).[51] In this model, the composite's thermal conductivity is a function of the NC core thermal conductivity (k_{NC}), ligand matrix thermal conductivity (k_m), volume fraction of the NC cores (V_{NC}), radius of the NC core (a), and core–ligand interface thermal conductance (h_c). We first perform a sensitivity analysis on the EMA model to understand the effect of each parameter on the thermal conductivity of NC assemblies (Figure S14). This analysis indicates that the composite thermal conductivity in the EMA model is most sensitive to k_m, which agrees with previous work.[14,15] In order to understand k_m and its role in thermal transport in NC assemblies, we calculate k_m and its uncertainty on the basis of the EMA model and our thermal conductivity data (Figure 2d).

Figure 2d shows that the k_m value of NCSLs increases with diameter (0.36–1.04 W m^{-1} K^{-1}) whereas the k_m value of the NCFs falls within a narrow range (0.13–0.20 W m^{-1} K^{-1}) with no obvious diameter dependence. This value for k_m in NCFs is similar to that of Pb oleate (0.13 W m^{-1} K^{-1}),[12] which consists of an OA molecule bound to a Pb atom and is representative of a ligand in our PbS NCFs. The thermal conductivity similarity between Pb oleate and the k_m value for NCFs indicates that the OA ligands are the bottleneck for the thermal transport in NCFs. In contrast, the k_m value for NCSLs increases 3-fold over our NC diameter range. This pronounced diameter dependence indicates that the structure of the ligand matrix in NCSLs must change with NC diameter in a manner that is obscured in NCFs. We attribute this size dependence in the ligand matrix thermal conductivity for NCSLs to variations in ligand order and interdigitation. While the slow growth of NCSLs allows for improved ligand order/interdigitation, the quality of this order/interdigitation is still limited by the NC surface curvature. Consequently, a set of NCSLs with varying NC diameters will still exhibit varying qualities of ligand order/interdigitation that can be traced to differences in NC surface curvature. This in turn leads to a ligand matrix thermal conductivity, k_m, that should increase with increasing diameter (decreasing surface curvature), as observed in Figure 2d. The lack of diameter dependence of k_m for NCFs likely occurs because the effect of the NC curvature is obscured by the disordered NC packing within NCFs. This effect of ligand order and interdigitation on thermal transport is once again analogous to thermal transport in polymers, where aligned chains improve heat conduction along the polymer chain axis.

We also used the minimum thermal conductivity model to calculate the thermal conductivity of the OA ligand matrix (Section VII of the Supporting Information). This model is known to successfully predict the thermal conductivity of amorphous materials (which are akin to the disordered ligand matrix within NCFs).[52−54] Inherent in the minimum thermal conductivity model is the assumption that the phonon MFP is

https://doi.org/10.1021/acs.nanolett.2c00544
Nano Lett. 2022, 22, 4669−4676

half of the phonon wavelength. Figure 2d shows that this model yields a reasonable match with k_m for NCFs, but a poor match for NCSLs. This poor match with NCSLs indicates that the average phonon MFP in NCSLs is larger than that in NCFs. Our collective modeling results and speed of sound data indicate that improved ligand alignment and interdigitation lead to improvements in both the phonon MFP and speed of sound to increase the overall NCSL thermal conductivity.

In summary, we report that long-range ordered PbS NCSLs have thermal conductivities and Young's moduli that are up to ~3 times higher than the corresponding properties in disordered PbS NCFs. The amount of this increase is similar to that achieved in cross-linked versus non-cross-linked iron oxide NCs,[15] but is particularly notable due to its differing mechanism. Unlike the strong covalent bonds formed in cross-linked iron oxide NCs, PbS NCSLs still feature vdW ligand−ligand interactions. This approach of using NC ordering to improve these properties is also much more generalizable across NC materials, since it does not require the high-temperature annealing process used in cross-linking iron oxide NCs. We identify improved ligand alignment and interdigitation in PbS NCSLs as the major contributor to the enhanced NC−NC interaction and thus higher thermal conductivity and Young's modulus. This conclusion is further confirmed by both thermal transport and mechanical modeling. Our work demonstrates the critical role of ligand alignment and interdigitation in determining the thermal transport and mechanical properties of NC assemblies.

■ ASSOCIATED CONTENT

Supporting Information

The Supporting Information is available free of charge at https://pubs.acs.org/doi/10.1021/acs.nanolett.2c00544.

Detailed descriptions, figures, and data on materials synthesis and characterization (TEM, SEM, profilometry, DSC, TGA), mechanical measurements/analysis, pair potential and coarse-grained modeling, atomistic molecular dynamics simulations, frequency domain thermoreflectance measurements, effective medium approximation modeling, minimum thermal conductivity modeling, and mass-spring modeling of coherent phonon transport in NCSLs (PDF)

■ AUTHOR INFORMATION

Corresponding Author

Robert Y. Wang − *School for Engineering of Matter, Transport & Energy, Arizona State University, Tempe, Arizona 85287, United States*; Email: rywang@asu.edu

Authors

Zhongyong Wang − *School for Engineering of Matter, Transport & Energy, Arizona State University, Tempe, Arizona 85287, United States;* Present Address: Department of Mechanical Engineering, University of Michigan, Ann Arbor, Michigan 48109, United States

Alexander D. Christodoulides − *Department of Mechanical Engineering, Carnegie Mellon University, Pittsburgh, Pennsylvania 15213, United States*

Lingyun Dai − *Department of Mechanical Engineering, Carnegie Mellon University, Pittsburgh, Pennsylvania 15213, United States*

Yang Zhou − *Department of Mechanical Engineering, University of Washington, Seattle, Washington 98195, United States*

Rui Dai − *School for Engineering of Matter, Transport & Energy, Arizona State University, Tempe, Arizona 85287, United States*

Yifei Xu − *School for Engineering of Matter, Transport & Energy, Arizona State University, Tempe, Arizona 85287, United States;* orcid.org/0000-0001-9787-5898

Qiong Nian − *School for Engineering of Matter, Transport & Energy, Arizona State University, Tempe, Arizona 85287, United States*

Junlan Wang − *Department of Mechanical Engineering, University of Washington, Seattle, Washington 98195, United States*

Jonathan A. Malen − *Department of Mechanical Engineering, Carnegie Mellon University, Pittsburgh, Pennsylvania 15213, United States;* orcid.org/0000-0003-4560-4476

Complete contact information is available at: https://pubs.acs.org/10.1021/acs.nanolett.2c00544

Author Contributions

R.Y.W. and J.A.M. conceived the study. Z.W. synthesized, fabricated, and characterized the samples under the supervision of R.Y.W. A.D.C. and L.D. performed the thermal transport experiments under the supervision of J.A.M. Y.Z. performed the nanoindentation experiments under the supervision of J.W. R.D. performed molecular dynamics simulation under the supervision of Q.N. Z.W. and Y.X. performed the heat capacity measurements and thermogravimetric analysis. Z.W. and A.D.C, analyzed the data and performed additional modeling. The manuscript was jointly written by all authors with the main contributions from Z.W. and R.Y.W. All authors have given approval to the final version of the manuscript.

Author Contributions

[⊥]Z.W. and A.D.C. contributed equally.

Notes

The authors declare no competing financial interest.

■ ACKNOWLEDGMENTS

This work was supported by the National Science Foundation CAREER program through award number DMR-1654337. We gratefully acknowledge the use of facilities within the Eyring Materials Center and the Nanofab at Arizona State University. We thank Lenore Dai of Arizona State University for allowing us to use her differential scanning calorimeter and thermogravimetric analyzer.

■ REFERENCES

(1) Choi, J. H.; Wang, H.; Oh, S. J.; Paik, T.; Sung, P.; Sung, J.; Ye, X.; Zhao, T.; Diroll, B. T.; Murray, C. B.; Kagan, C. R. Exploiting the Colloidal Nanocrystal Library to Construct Electronic Devices. *Science* **2016**, *352*, 205−208.

(2) Talapin, D. V.; Lee, J.-S.; Kovalenko, M. V.; Shevchenko, E. V. Prospects of Colloidal Nanocrystals for Electronic and Optoelectronic Applications. *Chem. Rev.* **2010**, *110*, 389−458.

(3) Boles, M. A.; Engel, M.; Talapin, D. V. Self-Assembly of Colloidal Nanocrystals: From Intricate Structures to Functional Materials. *Chem. Rev.* **2016**, *116*, 11220−11289.

(4) Kagan, C. R.; Murray, C. B. Charge Transport in Strongly Coupled Quantum Dot Solids. *Nat. Nanotechnol.* **2015**, *10*, 1013−1026.

(5) Kagan, C. R.; Lifshitz, E.; Sargent, E. H.; Talapin, D. V. Building Devices from Colloidal Quantum Dots. *Science* **2016**, *353*, aac5523.
(6) Liu, M.; Yazdani, N.; Yarema, M.; Jansen, M.; Wood, V.; Sargent, E. H. Colloidal Quantum Dot Electronics. *Nat. Electron.* **2021**, *4*, 548−558.
(7) Konstantatos, G.; Sargent, E. H. *Colloidal Quantum Dot Optoelectronics and Photovoltaics*; Cambridge University Press: 2013; pp 20−309.
(8) Lan, X.; Masala, S.; Sargent, E. H. Charge-Extraction Strategies for Colloidal Quantum Dot Photovoltaics. *Nat. Mater.* **2014**, *13*, 233−240.
(9) Ibánez, M.; Luo, Z.; Genc, A.; Piveteau, L.; Ortega, S.; Cadavid, D.; Dobrozhan, O.; Liu, Y.; Nachtegaal, M.; Zebarjadi, M.; et al. High-Performance Thermoelectric Nanocomposites from Nanocrystal Building Blocks. *Nat. Commun.* **2016**, *7*, 1−7.
(10) Zhang, H.; Son, J. S.; Jang, J.; Lee, J.-S.; Ong, W.-L.; Malen, J. A.; Talapin, D. V. Bi1-X Sb X Alloy Nanocrystals: Colloidal Synthesis, Charge Transport, and Thermoelectric Properties. *ACS Nano* **2013**, *7*, 10296−10306.
(11) Wang, R. Y.; Feser, J. P.; Lee, J.-S.; Talapin, D. V.; Segalman, R.; Majumdar, A. Enhanced Thermopower in Pbse Nanocrystal Quantum Dot Superlattices. *Nano Lett.* **2008**, *8*, 2283−2288.
(12) Ong, W. L.; Rupich, S. M.; Talapin, D. V.; McGaughey, A. J. H.; Malen, J. A. Surface Chemistry Mediates Thermal Transport in Three-Dimensional Nanocrystal Arrays. *Nat. Mater.* **2013**, *12*, 410−415.
(13) Begley, M. R.; Gianola, D. S.; Ray, T. R. Bridging Functional Nanocomposites to Robust Macroscale Devices. *Science* **2019**, *364*, No. eaav4299.
(14) Liu, M. L.; Ma, Y. Y.; Wang, R. Y. Modifying Thermal Transport in Colloidal Nanocrystal Solids with Surface Chemistry. *ACS Nano* **2015**, *9*, 12079−12087.
(15) Wang, Z. Y.; Singaravelu, A. S. S.; Dai, R.; Nian, Q.; Chawla, N.; Wang, R. Y. Ligand Crosslinking Boosts Thermal Transport in Colloidal Nanocrystal Solids. *Angew. Chem., Int. Ed.* **2020**, *59*, 9556−9563.
(16) Badia, A.; Singh, S.; Demers, L.; Cuccia, L.; Brown, G. R.; Lennox, R. B. Self-Assembled Monolayers on Gold Nanoparticles. *Chem. - Eur. J.* **1996**, *2*, 359−363.
(17) Terrill, R. H.; Postlethwaite, T. A.; Chen, C. H.; Poon, C. D.; Terzis, A.; Chen, A. D.; Hutchison, J. E.; Clark, M. R.; Wignall, G.; Londono, J. D.; Superfine, R.; Falvo, M.; Johnson, C. S.; Samulski, E. T.; Murray, R. W. Monolayers in Three Dimensions: Nmr, Saxs, Thermal, and Electron Hopping Studies of Alkanethiol Stabilized Gold Clusters. *J. Am. Chem. Soc.* **1995**, *117*, 12537−12548.
(18) Yang, Y.; Qin, H.; Peng, X. Intramolecular Entropy and Size-Dependent Solution Properties of Nanocrystal-Ligands Complexes. *Nano Lett.* **2016**, *16*, 2127−2132.
(19) Boles, M. A.; Talapin, D. V. Self-Assembly of Tetrahedral Cdse Nanocrystals: Effective "Patchiness" Via Anisotropic Steric Interaction. *J. Am. Chem. Soc.* **2014**, *136*, 5868−5871.
(20) Weidman, M. C.; Yager, K. G.; Tisdale, W. A. Interparticle Spacing and Structural Ordering in Superlattice Pbs Nanocrystal Solids Undergoing Ligand Exchange. *Chem. Mater.* **2015**, *27*, 474−482.
(21) Shen, S.; Henry, A.; Tong, J.; Zheng, R. T.; Chen, G. Polyethylene Nanofibres with Very High Thermal Conductivities. *Nat. Nanotechnol.* **2010**, *5*, 251−255.
(22) Henry, A. Thermal Transport in Polymers. *Annu. rev. heat transf.* **2014**, *17*, 485−520.
(23) Ma, H.; Tian, Z. Chain Rotation Significantly Reduces Thermal Conductivity of Single-Chain Polymers. *J. Mater. Res.* **2019**, *34*, 126−133.
(24) Luo, T.; Lloyd, J. R. Non-Equilibrium Molecular Dynamics Study of Thermal Energy Transport in Au-Sam-Au Junctions. *Int. J. Heat Mass Transfer* **2010**, *53*, 1−11.
(25) O'Brien, P. J.; Shenogin, S.; Liu, J.; Chow, P. K.; Laurencin, D.; Mutin, P. H.; Yamaguchi, M.; Keblinski, P.; Ramanath, G. Bonding-Induced Thermal Conductance Enhancement at Inorganic Heterointerfaces Using nanomolecular Monolayers. *Nat. Mater.* **2013**, *12*, 118−122.
(26) Majumdar, S.; Sierra-Suarez, J. A.; Schiffres, S. N.; Ong, W.-L.; Higgs, C. F.; McGaughey, A. J. H.; Malen, J. A. Vibrational Mismatch of Metal Leads Controls Thermal Conductance of Self-Assembled Monolayer Junctions. *Nano Lett.* **2015**, *15*, 2985−2991.
(27) Tian, Z.; Marconnet, A.; Chen, G. Enhancing Solid-Liquid Interface Thermal Transport Using Self-Assembled Monolayers. *Appl. Phys. Lett.* **2015**, *106*, 211602.
(28) Hostetler, M. J.; Stokes, J. J.; Murray, R. W. Infrared Spectroscopy of Three-Dimensional Self-Assembled Monolayers: N-Alkanethiolate Monolayers on Gold Cluster Compounds. *Langmuir* **1996**, *12*, 3604−3612.
(29) Ong, W.-L.; Majumdar, S.; Malen, J. A.; McGaughey, A. J. H. Coupling of Organic and Inorganic Vibrational States and Their Thermal Transport in Nanocrystal Arrays. *J. Phys. Chem. C* **2014**, *118*, 7288−7295.
(30) Talapin, D. V.; Shevchenko, E. V.; Kornowski, A.; Gaponik, N.; Haase, M.; Rogach, A. L.; Weller, H. A New Approach to Crystallization of Cdse Nanoparticles into Ordered Three-Dimensional Superlattices. *Adv. Mater.* **2001**, *13*, 1868−1871.
(31) Rogach, A. L.; Talapin, D. V.; Shevchenko, E. V.; Kornowski, A.; Haase, M.; Weller, H. Organization of Matter on Different Size Scales: Monodisperse Nanocrystals and Their Superstructures. *Adv. Funct. Mater.* **2002**, *12*, 653−664.
(32) Evers, W. H.; Nijs, B. D.; Filion, L.; Castillo, S.; Dijkstra, M.; Vanmaekelbergh, D. Entropy-Driven Formation of Binary Semiconductor-Nanocrystal Superlattices. *Nano Lett.* **2010**, *10*, 4235−4241.
(33) Vanmaekelbergh, D. Self-Assembly of Colloidal Nanocrystals as Route to Novel Classes of Nanostructured Materials. *Nano Today* **2011**, *6*, 419−437.
(34) Urban, J. J.; Talapin, D. V.; Shevchenko, E. V.; Murray, C. B. Self-Assembly of Pbte Quantum Dots into Nanocrystal Superlattices and Glassy Films. *J. Am. Chem. Soc.* **2006**, *128*, 3248−3255.
(35) Li, H.; Chen, D.; Li, L.; Tang, F.; Zhang, L.; Ren, J. Size- and Shape-Controlled Synthesis of Pbse and Pbs Nanocrystals Via a Facile Method. *CrystEngComm* **2010**, *12*, 1127−1133.
(36) Wang, Z.; Schliehe, C.; Bian, K.; Dale, D.; Bassett, W. A.; Hanrath, T.; Klinke, C.; Weller, H. Correlating Superlattice Polymorphs to Internanoparticle Distance, Packing Density, and Surface Lattice in Assemblies of Pbs Nanoparticles. *Nano Lett.* **2013**, *13*, 1303−1311.
(37) Choi, J. J.; Bealing, C. R.; Bian, K.; Hughes, K. J.; Zhang, W.; Smilgies, D.-M.; Hennig, R. G.; Engstrom, J. R.; Hanrath, T. Controlling Nanocrystal Superlattice Symmetry and Shape-Anisotropic Interactions through Variable Ligand Surface Coverage. *J. Am. Chem. Soc.* **2011**, *133*, 3131−3138.
(38) Weidman, M. C.; Nguyen, Q.; Smilgies, D.-M.; Tisdale, W. A. Impact of Size Dispersity, Ligand Coverage, and Ligand Length on the Structure of Pbs Nanocrystal Superlattices. *Chem. Mater.* **2018**, *30*, 807−816.
(39) Rupich, S. M.; Shevchenko, E. V.; Bodnarchuk, M. I.; Lee, B.; Talapin, D. V. Size-Dependent Multiple Twinning in Nanocrystal Superlattices. *J. Am. Chem. Soc.* **2010**, *132*, 289−296.
(40) Bealing, C. R.; Baumgardner, W. J.; Choi, J. J.; Hanrath, T.; Hennig, R. G. Predicting Nanocrystal Shape through Consideration of Surface-Ligand Interactions. *ACS Nano* **2012**, *6*, 2118−2127.
(41) Podsiadlo, P.; Krylova, G.; Lee, B.; Critchley, K.; Gosztola, D. J.; Talapin, D. V.; Ashby, P. D.; Shevchenko, E. V. The Role of Order, Nanocrystal Size, and Capping Ligands in the Collective Mechanical Response of Three-Dimensional Nanocrystal Solids. *J. Am. Chem. Soc.* **2010**, *132*, 8953−8960.
(42) Murray, C. B.; Kagan, C. R.; Bawendi, M. G. Self-Organization of Cdse Nanocrystallites into Three-Dimensional Quantum Dot Superlattices. *Science* **1995**, *270*, 1335−1338.
(43) Klokkenburg, M.; Houtepen, A. J.; Koole, R.; de Folter, J. W. J.; Erné, B. H.; van Faassen, E.; Vanmaekelbergh, D. Dipolar Structures

https://doi.org/10.1021/acs.nanolett.2c00544
Nano Lett. 2022, 22, 4669−4676

in Colloidal Dispersions of Pbse and Cdse Quantum Dots. *Nano Lett.* **2007**, *7*, 2931−2936.
(44) Li, R.; Bian, K.; Hanrath, T.; Bassett, W. A.; Wang, Z. Decoding the Superlattice and Interface Structure of Truncate Pbs Nanocrystal-Assembled Supercrystal and Associated Interaction Forces. *J. Am. Chem. Soc.* **2014**, *136*, 12047−12055.
(45) Hines, M. A.; Scholes, G. D. Colloidal Pbs Nanocrystals with Size-Tunable near-Infrared Emission: Observation of Post-Synthesis Self-Narrowing of the Particle Size Distribution. *Adv. Mater.* **2003**, *15*, 1844−1849.
(46) Lee, B.; Podsiadlo, P.; Rupich, S.; Talapin, D. V.; Rajh, T.; Shevchenko, E. V. Comparison of Structural Behavior of Nanocrystals in Randomly Packed Films and Long-Range Ordered Superlattices by Time-Resolved Small Angle X-Ray Scattering. *J. Am. Chem. Soc.* **2009**, *131*, 16386−16388.
(47) Malen, J. A.; Baheti, K.; Tong, T.; Zhao, Y.; Hudgings, J. A.; Majumdar, A. Optical Measurement of Thermal Conductivity Using Fiber Aligned Frequency Domain Thermoreflectance. *J. Heat Transfer* **2011**, *133*, 081601.
(48) Cahill, D. G. Analysis of Heat Flow in Layered Structures for Time-Domain Thermoreflectance. *Rev. Sci. Instrum.* **2004**, *75*, 5119−5122.
(49) He, J.; Kanjanaboos, P.; Frazer, N. L.; Weis, A.; Lin, X. M.; Jaeger, H. M. Fabrication and Mechanical Properties of Large-Scale Freestanding Nanoparticle Membranes. *Small* **2010**, *6*, 1449−1456.
(50) Zanjani, M. B.; Lukes, J. R. Size Dependent Elastic Moduli of Cdse Nanocrystal Superlattices Predicted from Atomistic and Coarse Grained Models. *Chem. Phys.* **2013**, *139*, 144702.
(51) Hasselman, D. P. H.; Johnson, L. F. Effective Thermal Conductivity of Composites with Interfacial Thermal Barrier Resistance. *J. Compos. Mater.* **1987**, *21*, 508−515.
(52) Xie, X.; Li, D.; Tsai, T.-H.; Liu, J.; Braun, P. V.; Cahill, D. G. Thermal Conductivity, Heat Capacity, and Elastic Constants of Water-Soluble Polymers and Polymer Blends. *Macromolecules* **2016**, *49*, 972−978.
(53) Xie, X.; Yang, K.; Li, D.; Tsai, T.-H.; Shin, J.; Braun, P. V.; Cahill, D. G. High and Low Thermal Conductivity of Amorphous Macromolecules. *Phys. Rev. B* **2017**, *95*, 035406.
(54) Cahill, D. G.; Watson, S. K.; Pohl, R. O. Lower Limit to the Thermal Conductivity of Disordered Crystals. *Phys. Rev. B* **1992**, *46*, 6131.

https://doi.org/10.1021/acs.nanolett.2c00544
Nano Lett. 2022, 22, 4669−4676